Nanoscale Phase Transitions Induced by Heat Spikes in Collision Cascades

H. Van Swygenhoven and A. Caro
Paul Scherrer Institute, 5232 Villigen, Switzerland
(Received 2 November 1992)

We present molecular dynamics computer simulations of heat spikes similar to those appearing in high energy collision cascades. We determine characteristics of the thermal transport and, by changing the energy density and the initial temperature of the substratum, we study the solid-to-liquid transition of the core of the spike. The change in volume associated with this transition generates a narrow density wave that drives the material to strains above the theoretical shear strength of a perfect crystal, becoming in this way a new possible mechanism of collective generation of dislocation loops.

PACS numbers: 61.80.−x, 05.70.Fh, 44.10.+i

Radiation damage cascades are ultrafast processes that drive ions and electrons in a solid far from equilibrium. In a time scale of a few psec the energy of the projectile is dissipated by nuclear and electronic collision, transformed into heat, and transported away by both ionic and electronic thermal conductivities. At the end of this process the crystalline structure is damaged. For pure metals, this damage is composed of both vacancies and self-interstitial atoms that may be isolated or in clusters that adopt different forms: dislocation loops, stacking fault tetrahedra, or voids [1].

The parameters which are relevant to understand the microscopic evolution of displacement cascades produced by high energy particle irradiation, such as the number and nature of defects produced or the amount of ion mixing, can be correctly studied using molecular dynamics computer simulations (MD). One of the most important results of MD is the prediction of cascade core melting [2]. In the resolidification process that follows, it is believed that the vacancies produced during the collisional phase cluster at the center of the heat spike, while the interstitials at the periphery may either cluster or freely migrate. Interstitial clustering is then an activated process, although MD simulations have shown that there is a tendency to cluster during the lifetime of the cascade. A recent MD simulation has suggested the possible existence of a collective mechanism, similar to dislocation punching near overpressurized gas bubbles, that would produce interstitial dislocation loops [3]. From the experimental point of view, there is some controversy concerning the possibility that interstitial clusters or dislocation loops are formed during the lifetime of the cascade in irradiations performed at temperatures below Stage I, where the interstitials are immobile [4–7].

In this work we perform simulations of the heat spike phase, after the collisional phase, i.e., when motion of all particles is thermal as opposed to ballistic, to study how the energy is removed and whether the melting picture of the core really implies a true phase transition. We also analyze the mechanisms responsible for vacancy clustering by simulating a heat spike in a crystal containing a high and uniform vacancy concentration. The simulations are done with a classical N-body potential for Cu based on the embedded atom model [8]. Equilibrium, elastic, and defect properties are known to be well described, but since our interest is to drive the system far from equilibrium, we have checked some other thermodynamic quantities. The predicted melting temperature at zero pressure is around 1400 K, to be compared with the experimental value of 1356 K; latent heat of melting is 0.10 eV/atom, while the experimental value is 0.135 eV/atom; the volume expansion under melting is 4.7%, while the experimental value is 5%; and finally the linear thermal expansion coefficient of the solid phase is 16.7×10^{-6} K^{-1}, while the experimental value is 17.0×10^{-6} K^{-1}. The very good agreement of all these quantities gives confidence in the reliability of the simulations for Cu. In addition, the role of the electronic thermal transport in this very fast process can be neglected in Cu as a first approximation, as discussed in Refs. [9,10].

The simulations are fully three-dimensional but we have chosen one-dimensional symmetry along the z direction for the thermal gradient in order to avoid the $1/r$ decrease of the fields (velocities, displacements). In this way much more numerical precision is obtained since waves preserve their amplitude. Also much larger samples (in the direction of propagation) can be simulated, decreasing the influence of boundary reflection. The simulations are done at constant volume, since the information of the expansion of the core region propagates out at the speed of sound, as discussed below. Damping in the $\pm z$ faces is applied to decrease as much as possible the intensity of reflected waves. The size of the simulation cell has been chosen to allow measurements of all quantities of interest before the reflected waves reach the spike.

We report results of simulations done on Cu samples containing 16000 atoms located on a bar of square section with dimensions $10a_0 \times 10a_0 \times 40a_0$, where a_0 is the lattice constant. For vacancy diffusion, samples containing 60000 atoms, $10a_0 \times 10a_0 \times 150a_0$, have been used. One-dimensional thermal spikes have been introduced at time zero with temperature gradients following a Gaussian profile along the z direction whose width equals $3a_0$ in all cases. Initial three-dimensional velocity vectors are obtained by properly scaling random numbers from a

Boltzmann distribution. Three types of spikes have been simulated; the first, with a peak energy of 1 eV/atom and initial sample temperature of 10 K, drives the system to temperatures always below the melting point (we call it solid spike). The second, with a peak energy of 2 eV/atom and initial temperature of 10 K, drives the sample well above the melting point only in the core region (solid-liquid spike). The last type of spike has a peak energy of 1 eV/atom and an initial temperature of 1500 K, with the whole sample in the liquid state (liquid spike).

Figure 1 shows the temperature profiles 1 psec after the creation of the spike (solid lines). In order to determine the heat conductivities in both the solid and liquid spikes, a nonlinear least squares fitting procedure with one free parameter in each case was used: Snapshots of temperature distributions $T(z_j,t_i)$ at times t_i, obtained by averaging the kinetic energy of all atoms in each (001) plane located at z_j, are used as a data base. A thermal conductivity proportional to $T^{-1/2}$ for the solid phase [11] and to T for the liquid phase [12] is obtained by minimizing the error between the analytic solution of the heat equation and this data base. These expressions correspond to lattice thermal transport in insulators. Other usual expressions for the solid ionic thermal conductivity at high temperature were used [11], but the $T^{-1/2}$ law better fits our data. Dashed lines in Fig. 1 represent the best analytic solutions for the solid (curve *a*) and the liquid (curve *c*) spikes. For the solid-liquid spike (curve *b*) the heat equation was solved using the previously found solid heat conductivity for the regions where $T < 1300$ K, the liquid conductivity for regions where $T > 1500$ K, and a thermal resistance to model the region between 1300 and 1500 K, where the solid-liquid interface is located, according to Ref. [13]: $dT/dt = \alpha \Delta T$, with α an adjustable parameter. The best fit shown in Fig. 1, which is poorer compared with cases *a* and *c*, clearly demonstrates that the role of the interface in the heat transport is not negligible. A proper treatment of the numerical solution of the heat transport in the presence of a moving interface with latent heat of melting, the Stefan problem [14], is out of the scope of the present work.

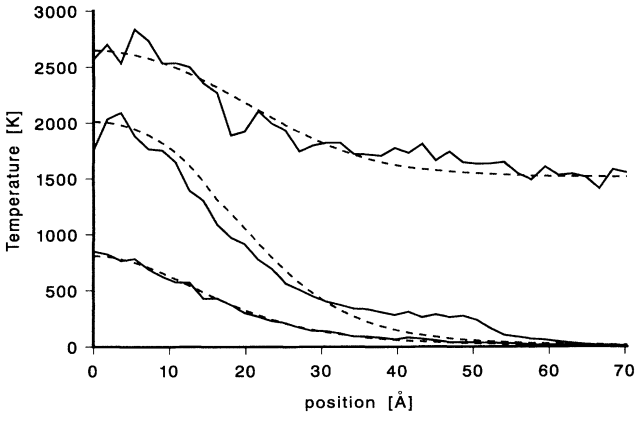

FIG. 1. Temperature profiles at 1 psec after the heat spike for the three simulations: The lowest curve corresponds to the solid heat spike, i.e., temperatures in the whole sample are below the melting point. The upper curve corresponds to the liquid spike: The whole sample is in the liquid phase. The intermediate curve corresponds to the solid-liquid case: The core of the spike undergoes a melting transition.

Figure 2 shows the temperature dependent values for the thermal conductivity: $K_{\text{solid-(001) direction}} = 0.012T^{-1/2}$, and $K_{\text{liquid}} = 0.046T$ both in W/cm K. If we compare these values with conductivities of standard dielectric insulators at room temperature (Tourmaline = 0.046; NaCl = 0.092; rock salt = 0.063; copper sulphate = 0.021; all in W/cm K) we see that the insulating copper under such large space and time temperature gradients (10^{14}–10^{15} K/sec and 10^{10} K/cm) behaves nevertheless as a normal heat conductor (unfortunately we are not aware of determinations of conventional steady state heat conductivity for this Cu potential). This result is not evident *a priori* because so small a system with so large a temperature gradient is far from the standard assumptions of thermodynamics. For comparison, it should be noted that the thermal conductivity of metallic copper at room temperature is 4.01 W/cm K, i.e., 2 orders of magnitude larger.

Quantitative knowledge of thermal conductivity is relevant for analytic calculations on heat spikes. Several papers in the literature use either constant values from experimental results for insulators, or different analytic forms for the temperature-dependent conductivity [15,16]. Precise knowledge of $K(T)$ would allow better analytic predictions, like for instance those made in the liquid drop model [17].

Figure 3 shows the atomic density at 1 psec as a function of distance from the center of the heat spikes. Figure 3(a) shows the curve for the solid spike. Thermal expansion is not apparent in the density scale reported. In

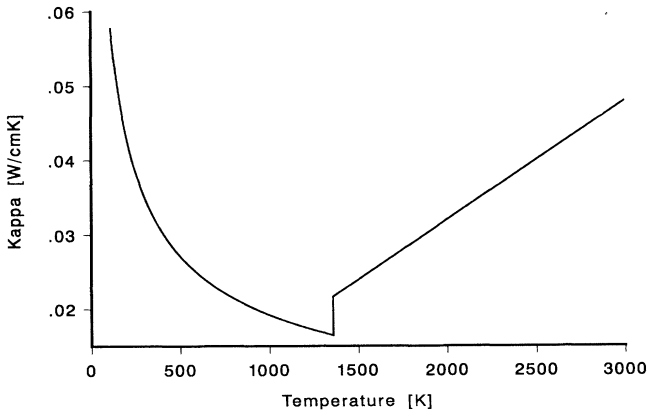

FIG. 2. Lattice thermal conductivity for the solid and liquid phases of Cu, as determined by the fitting procedure.

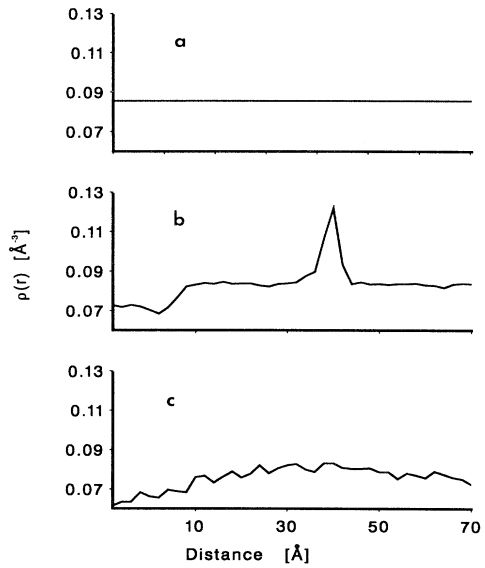

FIG. 3. Density profiles at 1 psec. (a) Solid spike; the energy density is 1 eV/atom and initial temperature 10 K. (b) Solid-liquid spike; energy density 2 eV/atom and initial temperature 10 K. (c) Liquid spike; energy density is 1 eV/atom and initial temperature 1500 K. These density profiles correspond to the temperature profiles reported in Fig. 1.

the liquid spike reported in Fig. 3(c), in contrast, the density reflects the presence of both a temperature gradient as well as a wide wave component originated in the sudden expansion. This density wave carries the displacement associated with the extra volume produced by the thermal expansion in the core of the heat spike. The thermal expansion is much larger than in the solid phase.

For the solid-liquid spike, Fig. 3(b) shows a well defined density peak that propagates away at the speed of sound (approximately 40 Å/psec), together with a mass depletion at the heat spike core. This wave, which only contains the compression peak, induces a net displacement of the sample behind them, like a dislocation in a one-dimensional Frenkel-Kontorova model [18]. The magnitude of this displacement is related to the volume expansion produced in the melting transition, as well as the liquid thermal expansion contribution. Quantitative evaluation of the deformation carried away by the density wave shows that the net displacement is approximately 2 Å. A volume expansion of 5% under melting of a region extending to 20 Å from the center of the spike gives a contribution of half of this amount. The remaining displacement is due to liquid thermal expansion. However, these two components have a different time scale, namely, the expansion under melt happens on a much shorter time scale, producing a narrow wave front with significantly higher strain, as can be concluded by comparing the liquid [curve 3(c)] and the solid-liquid [curve 3(b)] spikes: In fact, the maximum strain in this wave is 10% of the interplanar spacing which in terms of stress represents 0.1 of the bulk modulus B.

We believe that the qualitative difference between the density curves for liquid and solid-liquid spikes, namely, the creation of a quite narrow density peak, is a signature of the melting transition, providing a strong additional argument to the picture of cascade core melting. Previous justifications were based on the pair correlation function, the atomic mobility, and the density of those atoms in the core region, in agreement with the values corresponding to the liquid phase [2].

An important consequence of the existence of this density wave concerns the mechanism of defect production. Recent MD simulations have shown that point defects produced by cascades are the result of either the ejection of interstitial atoms from the core of the cascades via replacement collision sequences (RCS) [2], or a new cooperative mechanism not related to RCS but analogous to dislocation loop punching, originally proposed to explain overpressurized gas bubble growth [19]. At present some controversy arises due to the high pressures that are necessary to activate this mechanism that are not believed to exist in collision cascades. Calculations on the core overpressure produced by heat, and the shock wave that ensues, neglecting the melting transition, have been reported some time ago [20]. By inspection of Fig. 3, we conclude that in a real situation an additional mechanism related to volume expansion under melting may be responsible for a significant increase in pressure. In fact the stress we obtained in our simulations, $0.1B$, corresponds to a pressure of 0.22μ, where μ is the shear modulus (c_{44}). This stress is comparable to the theoretical limit to induce permanent plastic deformation, i.e., 0.2μ [1]. We conclude then that radiation damage cascades in real materials, which involve energy densities comparable to those used in this work, may induce such high stresses provided its size is large enough so that 5% of its expansion generates the required strain, and its geometry helps the creation of a narrow wave front with shear components. These conditions are not necessarily fulfilled in all materials because they depend on the melting temperature, energy density deposited in the collisional phase, and subcascade formation energy. It is important to point out that the symmetry of our simulation prevents the creation of a dislocation loop because the generated wave only has uniaxial compression, but in a general case, without symmetry constraints, both uniaxial and shear components are present. Also important to note is the fact that using conventional continuum calculations this prediction could not have been made because the detailed description of the strain field as a function of $\mathbf{r}$ and t during the phase transition is unknown. Only a full MD simulation provides this type of microscopic information.

Figure 4 shows the final vacancy configuration, 6 psec after the heat spike, in a large sample prepared with an initial 4% uniform vacancy concentration at a tempera-

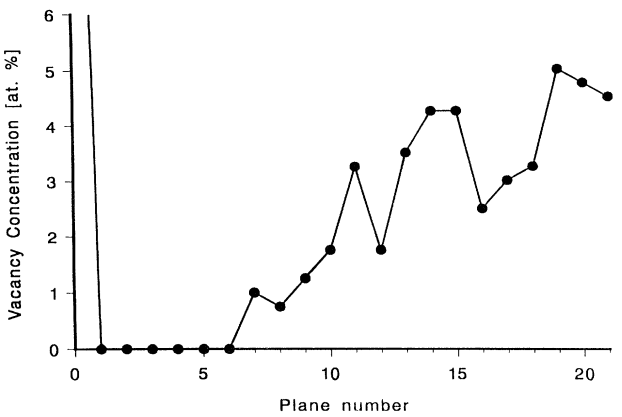

FIG. 4. Vacancy concentration at the end of the heat spike ($t=6$ psec). Initial concentration is 4%. At the origin the concentration is 100%, i.e., an atomic plane has disappeared.

ture of 10 K, and heated up with a spike of 2 eV/atom, i.e., the same conditions as our previous solid-liquid spike. For the energy density used in this simulation, the temperature profile is such that the melting temperature is located at 20 Å for $t=0$, while at $t=0.5$ psec it is located at 18 Å, and at $t=2$ psec it is located at 12 Å. In terms of numbers of (001) lattice planes, these correspond to 11, 10, and 7 planes, respectively. This figure shows a complete vacancy depletion of the first six layers and a smooth concentration gradient that extends as far as eighteen planes, well inside the solid phase. This indicates that the driving force for vacancy migration cannot be associated solely with the interface motion or with the thermal gradient, but with both of them. Diffusion in the solid phase at this vacancy concentration is strongly enhanced by vacancy-vacancy interaction, as shown in Ref. [21]. Within the spike lifetime, the vacancy diffusion is extremely efficient, in such a way that in our simulation a full plane of vacancies was created at the center, giving a 100% vacancy concentration, or, in other words, the disappearance of an atomic plane.

In summary we have provided a quantitative evaluation of thermal conductivity and qualitatively estimated the role of the solid-liquid interface in thermal transport inside a cascade. We have observed a clear signature of a nanoscale phase transition as the creation of a density wave that carries away a plastic deformation equal to the extra volume produced by melting, and we have observed that this narrow density wave, added to the well known shock wave produced by the thermal expansion, drives the system to dynamical stresses above the theoretical limit for permanent plastic deformations, becoming in this way a possible collective mechanism for the formation of dislocation loops by radiation damage cascades. Finally, the temperature gradient together with the solid-liquid interface motion appear to be extremely efficient to provide a driving force for vacancy migration. Whether the moving solidification interface or the temperature gradient inside the melt gives the major contribution to this driving force is not clearly answered by our simulations.

One of us (H.V.S.) gratefully acknowledges the Fonds National Suisse de la Recherche Scientifique for financial support through Marie Heim-Voegtlin fellowship. This work was partially supported by the Fonds National Suisse de la Recherche Scientifique, Grant No. 20-28978.90.

[1] See J. P. Hirt and J. Lothe, in *Theory of Dislocations* (Wiley, New York, 1982).
[2] T. Diaz de la Rubia, R. S. Averback, R. Benedek, and W. E. King, Phys. Rev. Lett. **59**, 1930 (1987); T. Diaz de la Rubia, R. S. Averback, H. Hsieh, and R. Benedek, J. Mater. Res. **4**, 579 (1989).
[3] T. Diaz de la Rubia and M. Guinan, Phys. Rev. Lett. **66**, 2766 (1991).
[4] D. N. Seidman, R. S. Averback, and R. Benedek, Phys. Status Solidi (b) **144**, 85 (1987).
[5] P. Ehrhart and R. S. Averback, Philos. Mag. A **60**, 283 (1989).
[6] B. von Guerard, D. Grasse, and J. Peisl, Phys. Rev. Lett. **44**, 262 (1980).
[7] Y. Shimomura, M. W. Guinan, H. Fukushima, P. A. Hahn, and M. Kiritani, J. Nucl. Mater. **155-157**, 1181 (1988).
[8] S. M. Foiles, M. I. Baskes, and M. S. Daw, Phys. Rev. B **33**, 7983 (1986).
[9] A. Caro and M. Victoria, Phys. Rev. A **40**, 2287 (1989).
[10] S. Proennecke, A. Caro, M. Victoria, T. Diaz de la Rubia, and M. W. Guinan, J. Mater. Res. **6**, 483 (1991).
[11] J. M. Ziman, in *Principles of the Theory of Solids,* (Cambridge Univ. Press, Cambridge, 1972), p. 243.
[12] N. H. March, in *Liquid Metals* (Cambridge Univ. Press, Cambridge, 1990).
[13] H. Biloni, in *Physical Metallurgy,* edited by P. Haasen and R. W. Cahn (North-Holland, Amsterdam, 1983), p. 480.
[14] J. Crank, in *Free and Moving Boundary Problems* (Clarendon, Oxford, 1984).
[15] P. Sigmund and M. Szymonski, Appl. Phys. A **33**, 141 (1984).
[16] R. Kelly, Radiat. Eff. **32**, 91 (1977).
[17] M. Alurralde, A. Caro, and M. Victoria, J. Nucl. Mater. **183**, 33 (1991).
[18] J. Frenkel and T. Kontorova, Phys. Z. Sowj. **13**, 1 (1938).
[19] W. G. Wolfer, Philos. Mag. A **58**, 285 (1988).
[20] M. Guinan, J. Nucl. Mater. **53**, 171 (1974).
[21] V. G. Kapinos, Yu. N. Osetskii, and P. A. Platonov, J. Nucl. Mater. **184**, 221 (1991).